High Temperature Hydrothermal Synthesis of Rare-Earth Titanates: Synthesis and Structure of RE5Ti4O15(OH) (RE = La, Er), Sm3TiO5(OH)3, RE5Ti2O11(OH) (RE = Tm-Lu) and Ce2Ti4O11

SCHOLARONE™
Manuscripts

High Temperature Hydrothermal Synthesis of Rare-Earth Titanates: Synthesis and Structure of $RE_5Ti_4O_{15}(OH)$ (RE = La, Er), $Sm_3TiO_5(OH)_3$, $RE_5Ti_2O_{11}(OH)$ (RE = Tm-Lu) and $Ce_2Ti_4O_{11}$

Kyle Fulle, Liurukara D. Sanjeewa, Colin D. McMillen, Joseph W. Kolis*

Department of Chemistry and Center for Optical Materials Science and Engineering Technologies (COMSET), Clemson University, Clemson, South Carolina 29634-0973, USA

ABSTRACT

Reactions of rare-earth oxides with TiO_2 were performed in high temperature (650-700˚C) hydrothermal fluids. Two different mineralizer fluids were examined, 20 M KOH and 30 M CsF, and their respective products analyzed. When concentrated KOH fluids were used, single crystals of a variety of new OH^- containing species were isolated and structurally characterized: $RE_5Ti_4O_{15}(OH)$ (RE = La, Er) **I**, $Sm_3TiO_5(OH)_3$ **II** and $RE_5Ti_2O_{11}(OH)$ (RE = Tm-Lu) **III**. $La_5Ti_4O_{15}(OH)$ **I** crystallizes in the orthorhombic space group *Pnnm* with unit cell dimensions of a = 30.5152(12) Å, b = 5.5832(2) Å, c = 7.7590(3) Å and V = 1321.92(9) Å^3, Z = 4. $Sm_3TiO_5(OH)_3$ **II** crystallizes in the monoclinic space group $P2_1/m$ with unit cell parameters of a = 5.6066(2) Å, b = 10.4622(4) Å, c = 6.1258(2) Å and β = 104.7390(10)°, V = 347.50(2) Å^3, Z = 2. $Lu_5Ti_2O_{11}(OH)$ **III** crystallizes in the monoclinic space group $C2/m$ with unit cell dimensions of a = 12.1252(9) Å, b = 5.8243(4) Å, c = 7.0407(5) Å, β = 106.939(3)° and V = 475.65(6) Å^3, Z = 2. When concentrated fluoride solutions are used, mostly $RE_2Ti_2O_7$ type compounds were isolated in either cubic or monoclinic phases. In the case of cerium, $Ce_2Ti_4O_{11}$ **IV** was isolated that crystallizes in the monoclinic space group *C2/c* with unit cell parameters of a = 13.6875(7) Å, b = 5.0955(3) Å, c = 12.8592(7) Å, β = 108.964(2)° and V = 848.18(8) Å^3, Z = 4. The synthesis, structural characterization, and supporting characterization are reported for all

compounds. The work highlights the complementary nature of hydroxide and fluoride fluids in studying the reactivity of refractory oxides.

1. Introduction

Rare earth (RE = La-Lu, Y) titanates have a long history of study, particularly those exhibiting $RE_2Ti_2O_7$ pyrochlore-type structures.[1,2] These receive considerable attention due to their unusual magnetic behavior including spin frustration and spin ice behavior.[3–12] The rare earth titanates have also been investigated for several other potential properties and applications, including ionic conductivity, actinide immobilization and high temperature piezoelectricity.[13–21]

While the cubic pyrochlore has become the most well-known and studied structure type of the rare earth titanates,[1,2,16] other polymorphs of the $RE_2Ti_2O_7$ formulation are also known, particularly those of the early rare earths (La, Pr, Nd) with polar biaxial structures.[19,21–26] In addition there are rare earth titanates, such as $RETiO_3$,[27] RE_2TiO_5 (RE = Yb, Dy, Gd, Sm, Nd, La),[28–31] $La_4Ti_3O_{12}$,[32,33] and $CeTi_2O_6$,[34] in the literature that display complex three dimensional (3-D) frameworks with uses ranging from photocatalysts to ceramics for electronic circuits. Given the breadth of structural diversity in the rare earth titanates and their significance in materials applications, we felt it was useful to explore the structural chemistry more fully by employing an alternative synthetic approach, specifically the high temperature hydrothermal method. Due to the high melting points of the rare-earth oxides (>2000 °C) and the tendency of Ti^{4+} oxides to become reduced at high reaction temperatures to form defect-containing structures,[35,36] the exploration of relatively lower reaction temperature techniques is of interest. Many solid-state techniques employed in the synthesis of rare earth titanates lead to formation of powder or poor single crystal quality due to oxygen defects, thermal strain and contaminations

from crucibles at high temperatures. The need for high quality single crystals is essential to study, for example, subtle but important effects such as site symmetry upon ordering in applied magnetic fields and complex frustrated structures.

In this regard the exploration of hydrothermal synthesis methods is of interest.[37–40] We found that suitable conditions can be developed for the synthesis of otherwise extremely refractory metal oxides.[41–45] A key component of the crystal growth of refractory oxides is the identity of the mineralizer. In many cases, concentrated hydroxides are suitable but often the use of fluorides is required to solubilize extremely refractory oxides.[43] In this work both hydroxide and fluoride mineralizers were examined. Recently, our group investigated the high temperature hydrothermal synthesis of rare earth containing niobates, RENbO$_4$ (RE = La-Lu, Y).[46] These crystals were grown from high concentrations (30 M) of potassium hydroxide in sealed silver ampoules with crystal sizes on the order of 3 mm/edge. This methodology was extended to the RE_2O_3-TiO$_2$ system (RE = La - Lu) in this paper, to investigate the descriptive reaction chemistry of rare-earth titanates in hydrothermal fluids grown at temperatures much lower than those utilized by traditional melt or flux techniques.

The goal of this effort is twofold. First, we wish to determine if useful known rare earth titanate oxides (e.g. pyrochlores) can be synthesized using hydrothermal techniques and if the method can lead to high quality, defect free single crystals. Second, we wish to determine if *new* phases can be synthesized and characterized that are unique to this methodology. Herein, we report a systematic investigation of reactions of all the lanthanide oxides with TiO$_2$ in high temperature hydrothermal fluids. We found a variety of species, ranging from well-known cubic pyrochlores to a series of new rare earth titanate hydroxides. The chemistry of this series of compounds is summarized and the single crystal structures of the new species La$_5$Ti$_4$O$_{15}$(OH) **I**,

$Sm_3TiO_5(OH)_3$ **II**, $Lu_5Ti_2O_{11}(OH)$ **III** and $Ce_2Ti_4O_{11}$ **IV** are described. Additionally, the role of the mineralizer was examined by comparing products using concentrated hydroxide fluids to those obtained from concentrated fluorides. The structural classes appear to be a function of the size of the rare-earth ion as well. The synthetic techniques employed, crystal structure and other analysis will be discussed. Several of the compounds have unusual structural relationships with some seemingly unrelated materials and these structural relationships are additionally discussed.

2. Experimental section

2.1. Hydrothermal crystal growth and reagents

A high-temperature (700 °C) hydrothermal technique was employed to synthesize new titanate-based rare earth (*RE*) oxide and oxy-hydroxide materials. Representative crystals of the reported compounds are shown in Figure 1. In each reaction, approximately 0.2 g of reactants with 0.4 mL of either 20 M KOH or 30 M CsF mineralizer fluids were used. In the case of $Ce_2Ti_4O_{11}$, a 6 M CsF mineralizer was susbsequently used to achieve the best quality single crystals after preliminary identification. All reactions were performed in 6.4 cm long silver ampoules with an outer diameter of 0.64 cm. The weld-sealed silver ampoules were loaded into a Tuttle cold-seal style autoclave that was filled with distilled water at 80% of free volume to provide suitable counter pressure. The autoclave was heated to 700 °C for seven days at a typical pressure of 150 MPa. After cooling to room temperature, the crystals were retrieved by filtering the product and washing with deionized water. In most cases the final products were large, uniform single crystals with sizes ranging from 0.5-1 mm, although crystals as large as several millimeters could be obtained in some cases. Occasionally, some additional powder consisting of rare-earth oxide or oxy-hydroxide accompanied the product, but always as a minor impurity. The

stoichiometric ratios and amounts used are given in detail under the Supplementary Information

(SI). The chemicals used in this study were used as received, without further purification: La_2O_3

(Alfa Aesar, 99.999%), Ce_2O_3 (CERAC, 99.9%), Pr_2O_3 (Alfa Aesar, 99.99%), Nd_2O_3 (Alfa

Aesar, 99.99%), Sm_2O_3 (Alfa Aesar, 99.99%), Eu_2O_3 (HEFA Rare Earth, 99.9%), Gd_2O_3 (HEFA

Rare Earth, 99.9%), Tb_4O_7 (HEFA Rare Earth, 99.9%), Dy_2O_3 (STREM, 99.9%), Ho_2O_3 (HEFA

Rare Earth, 99.9%), Er_2O_3 (Alfa Aesar, 99.99%), Tm_2O_3 (HEFA Rare Earth, 99.9%), Yb_2O_3

(HEFA Rare Earth, 99.99%), Lu_2O_3 (Alfa Aesar, 99.9%), TiO_2 (Alfa Aesar, 99.99%), CsF (Alfa

Aesar, 99.9%), $CsOH \cdot xH_2O$ (Alfa Aesar, 99.9%) and KOH (Alfa Aesar, 99.98%).
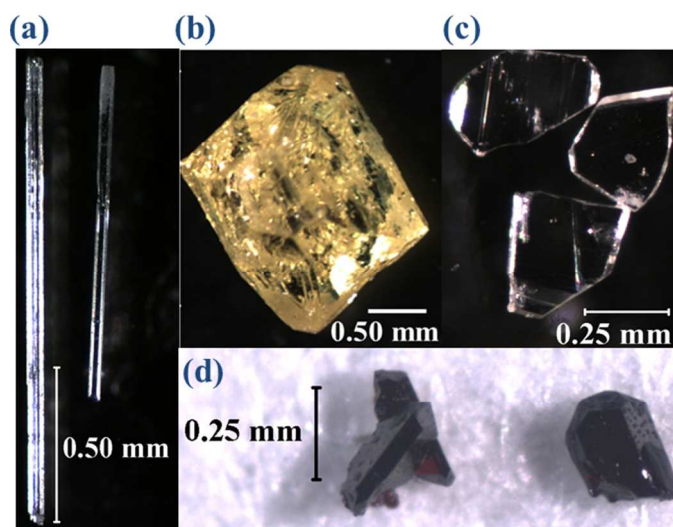
Figure 1. Typical examples of hydrothermally grown single crystals **(a)** $La_5Ti_4O_{15}(OH)$ **(b)** $Sm_3TiO_5(OH)_3$ **(c)** $Lu_5Ti_2O_{11}(OH)$ and **(d)** $Ce_2Ti_4O_{11}$.

2.2. Structure determination and supporting characterization

Single crystal structure characterization was conducted using a Bruker D8 Venture single

crystal diffractometer with an Incoatec Mo Kα microfocus source and Photon 100 CMOS

detector. Data were collected at room temperature using phi and omega scans, and subsequently

processed and scaled using the Apex3 (SAINT and SADABS) software package.[47] Space group

determinations were made based on the systematic absences. The structures were solved by

direct methods and refined to convergence by full-matrix least squares on F^2 using the SHELXTL software suite.[48] All non-hydrogen atoms were refined anisotropically. Hydrogen atom locations were identified from the difference electron density map and their occupancies were set to conform to realistic geometries in accordance with electroneutrality. In the case of $Lu_5Ti_2O_{11}(OH)$, *PLATON*[49] was used to determine the twin law and further details on the structure refinement are provided in the SI. The results of the structure refinements are presented in Table 1, and selected bond lengths and bond valence sum (BVS) calculations are given in the SI, Tables SI 1-5.[50,51] Phase purity was studied using powder X-ray diffraction (PXRD) (SI, Figures SI 1-4). The PXRD data were collected using a Rigaku Ultima IV diffractometer equipped with Cu Kα radiation (λ = 1.5406 Å) in the range of 5-65° in 2θ with a scan speed of 0.25 degrees per minute and a step size of 0.02°.

Single crystal Raman spectroscopy was used to confirm the presence of the hydroxide groups in the **I**, **II** and **III** structure types. The Raman spectra of compounds are displayed in Figure SI 5. Raman spectra were collected using an Olympus IX71 inverted microscope with a 20× objective lens coupled to a TRIAX 552 spectrometer equipped with a thermoelectrically cooled CCD detector (Andor Technology, Model DU420A-BV) operating at −60 °C were used. Single crystal specimens were used in the data collection and an Argon ion laser (Innova 100, Coherent) was used to excite the Raman signal with 514.5 nm light in a 180° backscattering geometry. Data were collected with a laser output power from 100 to 200 mW with a 2 min integration time. Additionally, the elemental compositions of all the reported compounds were investigated using energy dispersive X-ray analysis (EDX) via a 3400N Oxford variable-pressure scanning electron microscope equipped with a tungsten filament operating at a resolution of 3 nm under 20 kV potential, Table SI 6.

Table 1 Crystallographic data of $La_5Ti_4O_{15}(OH)$, $Sm_3TiO_5(OH)$, $Lu_5Ti_2O_{11}(OH)$, and $Ce_2Ti_4O_{11}$ determined by single crystal X-ray diffraction. Further details of the crystal structure investigations may be obtained from FIZ Karlsruhe on quoting the deposition number CSD-numbers 433895-433899

	$La_5Ti_4O_{15}(OH)$ I	$Sm_3TiO_5(OH)_3$ II	$Lu_5Ti_2O_{11}(OH)$ III	$Ce_2Ti_4O_{11}$ IV
formula weight (g/mol)	1143.16	629.97	1163.62	647.84
crystal system	orthorhombic	monoclinic	monoclinic	monoclinic
space group, Z	$Pnnm$ (no. 58), 4	$P2_1/m$ (no. 11), 2	$C2/m$ (no. 12), 2	$C2/c$ (no. 15), 4
Temperature (K)	298(2)	298(2)	298(2)	297(2)
Crystal size (mm)	0.27 x 0.04 x 0.03	0.04 x 0.05 x 0.05	0.05 x 0.06 x 0.06	0.05 x 0.06 x 0.06
a, Å	30.5152(12)	5.6066(2)	12.1252(9)	13.6875(7)
b, Å	5.5832(2)	10.4622(4)	5.8243(4)	5.0955(3)
c, Å	7.7590(3)	6.1258(2)	7.0407(5)	12.8592(7)
β, º	----	104.7390(10)	106.939(3)	108.964(2)
volume (Å^3)	1321.92(9)	347.50(2)	475.65(6)	848.18(8)
D_{calc} (g/cm^3)	5.744	6.021	8.125	5.073
abs. coeff. (mm^{-1})	18.140	26.085	53.027	14.147
F(000)	2008	550	992	1168
Tmax, Tmin	1.0000, 0.6321	1.000, 0.7912	1.0000, 0.5101	1.0000, 0.7998
Θ range for data	2.709-26.498	3.439-28.309	3.024-26.498	3.147-26.490
Reflections collected	8894	8323	2796	7614
data/restraints/parameters	1452/0/129	914/2/69	552/48/58	874/0/78
final R [$I > 2\sigma(I)$] R1, wR2	0.0195, 0.0464	0.0149, 0.0311	0.0294, 0.0701	0.0180, 0.0476
final R (all data) R1, wR2	0.0203/0.0468	0.0159, 0.0313	0.0349, 0.0720	0.0203, 0.0747
goodness-of-fit on F^2	1.177	1.261	1.368	1.176
largest diff. pk/hl, e/ Å^3	1.124/-2.480	1.131/-1.048	1.282/-3.536	0.846/-1.135

3. Results and discussion

3.1. Synthesis and phase distribution

The title compounds were synthesized by employing a high temperature hydrothermal method with 20 M KOH and 30 M CsF as mineralizers. In general, at lower temperatures ($T <$ 600 °C) the rare earth oxyhydroxide (REO(OH)) and trihydroxide (RE(OH)$_3$) species are the thermodynamically dominating products regardless of mineralizer choice. Thus, use of higher temperature regimes ($T \geq$ 650 °C) is essential to achieve new chemistry with RE_2O_3 and TiO_2. The product distribution across the rare-earth oxide series in this study is summarized in Scheme 1. A wide variety of products resulted depending upon the mineralizer and the size of the rare earth cation. It is important to mention that, for all the reactions, we maintained the stoichiometry between RE_2O_3 and TiO_2 at 1:2. However, in some cases stoichiometric reactions of the precursors were subsequently used to prepare the target compounds in a higher yield after the preliminary reactions.

The 20 M KOH reaction series has a very complicated phase distribution. The first compound isolated with the reaction between La_2O_3 and TiO_2 with 20 M KOH, $La_5Ti_4O_{15}$(OH) **I**, represents a new structure type. Needle-shaped $La_5Ti_4O_{15}$(OH) single crystals (Figure 1a) were obtained in high yield and phase purity was further confirmed by PXRD, Figure SI 1. However, this phase did not persist across the other lanthanide ions to form other analogs of $La_5Ti_4O_{15}$(OH) except in the case of $Er_5Ti_4O_{15}$(OH), Table SI 1. Reactions of Pr_2O_3 and Nd_2O_3

with TiO_2 resulted $Pr_2Ti_2O_7$ and $Nd_2Ti_2O_7$ which crystalize in monoclinic space group $P2_1$.[26,52] In a similar fashion, reactions from Gd_2O_3 to Ho_2O_3 produced cubic pyrochlore-type $RE_2Ti_2O_7$ structures.[1,2] In the case of Sm, yellow crystals of $Sm_3TiO_5(OH)_3$ **II** were isolated (~ 2 mm, Figure 1b) with a small amount of $Sm(OH)_3$ as a side product (Figure SI 2). Compound **II** was found to be isostructural with the $RE_3MO_5(OH)_3$ ($M = V^{+4}$, Ge^{+4}) structure type (see structure discussion of $Sm_3TiO_5(OH)_3$). The reactions from Tm_2O_3 to Lu_2O_3 with TiO_2 with 20 M KOH resulted $RE_2Ti_2O_{11}(OH)$ phases which share some similar structural features with rare-earth molybdates, ruthenates and rhenates ($RE_5X_2O_{12}$, X = Mo, Ru, Re) reported in the literature.[53–57] The synthesis of $Lu_5Ti_2O_{11}(OH)$ was accomplished in good yield, producing thick colorless crystals with well-defined edges (Figure 1c). The phase formation of $Tm_5Ti_2O_{11}(OH)$ and $Yb_5Ti_2O_{11}(OH)$ were confirmed only using PXRD (Figure SI 3), and no ambiguous reflections from additional phases were observed. In general, it appears that the stability of the monoclinic and cubic pyrochlore phases predominates in the phase space, and the new hydroxide-containing species we observe occur at the largest and smallest lanthanide size extremes, and the transition points (for example, Sm) between $RE_2Ti_2O_7$ polymorphs.

The reaction between Ce_2O_3 and TiO_2 with 20 M KOH only produced CeO(OH), even at 700 °C. As a result of that, we investigated the reactivity of RE_2O_3 and TiO_2 in the presence of 30 M CsF mineralizer and the product distribution is also presented in Scheme 1. Primarily, the use of 30 M CsF with stoichiometric ratio of 1:2 between RE_2O_3 (RE = Gd-Lu) and TiO_2 resulted cubic pyrochlore $RE_2Ti_2O_7$ structures with average crystal size of ~ 0.5 mm. The formation of monoclinic $P2_1$ $RE_2Ti_2O_7$ compounds was also observed with larger rare earth oxide cations such as La, Pr and Nd, which is somewhat similar to the reaction chemistry of 20 M KOH. Interestingly, the reaction between Ce_2O_3 and TiO_2 with 30 M CsF resulted dark orange/red

single crystals (Figure 1d) of $Ce_2Ti_4O_{11}$ **IV** which is isostructural with $Nd_2Ti_4O_{11}$ crystals grown by chemical transport at high temperature (1000°C) with the aid of chlorine gas as a transport catalyst.[58] The best quality crystals of compound **IV** were synthesized using 6 M CsF with higher yield, Figure SI 4. A very limited number of well-characterized cerium titanate single crystals are reported up to date, and in particular, the brannerite-type ($CeTi_2O_6$) cerium titanate is of interest as a catalyst.[59,60] Changing the rare-earth oxide to Sm_2O_3 and Eu_2O_3 did not produced any oxide materials, but rather resulted in the formation of rare earth fluoride compounds, $CsRE_2F_7$.[61] Highly concentrated fluoride solutions appear to be an effective route to obtain refractory oxide materials that do not contain hydroxide groups. This complements the studies with extremely high concentrated hydroxide that were very useful in obtaining a variety of new structure types.

The concept of using a fluoride-containing solution to grow crystals of oxide phases is interesting, though not unprecedented. In general, we have found that the tetravalent metal oxides are often more effectively solubilized by fluoride than hydroxide,[43] providing the key first step to the hydrothermal reactivity and synthesis. We postulate that a fluoride intermediate may be formed, that is subsequently hydrolyzed by the hydrothermal water and crystallizes the oxide. The versatility of the hydrothermal technique to support interchangeable mineralizer schemes thus makes it a valuable tool for the preparation of high quality single crystals of targeted materials (such as the pyrochlores) as well as engaging in exploratory chemistry.
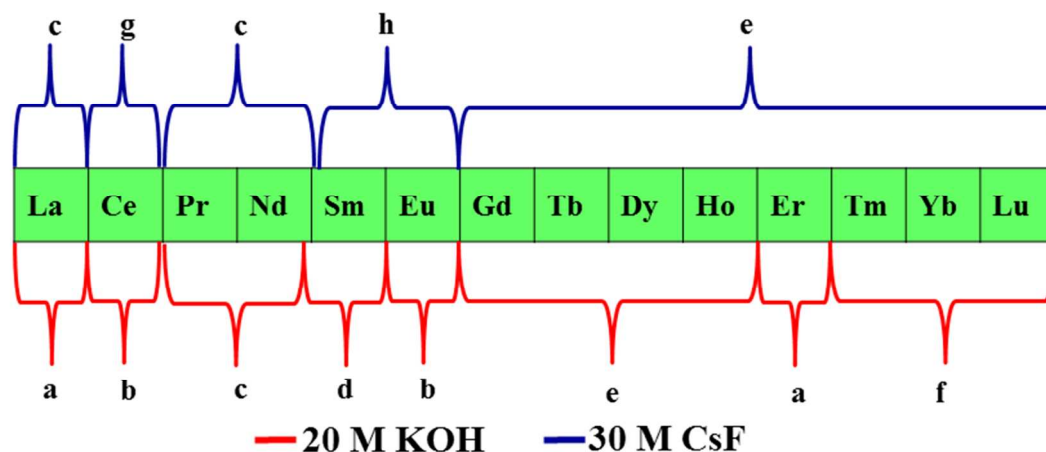
Scheme 1. Product distribution (a-h) of the hydrothermal reaction (650-700 ^{0}C) over the mineralizers of 20 *M* KOH and 30 *M* CsF: (a) *RE*$_5$Ti$_4$O$_{15}$(OH); (b) *RE*O(OH); (c) *RE*$_2$Ti$_2$O$_7$-*P*2$_1$; (d) *RE*$_3$TiO$_5$(OH)$_3$; (e) *RE*$_2$Ti$_2$O$_7$-cubic pyrochlore; (f) *RE*$_5$Ti$_2$O$_{11}$(OH); (g) *RE*$_2$Ti$_4$O$_{11}$; (h) Cs*RE*$_2$F$_7$.

3.2. Crystal structure of *RE*$_5$Ti$_4$O$_{15}$(OH) (*RE*= La and Er)

La$_5$Ti$_4$O$_{15}$(OH) (**1**) and Er$_5$Ti$_4$O$_{15}$(OH) are isostructural and crystallize in the orthorhombic crystal system in space group *Pnnm* (no.58). The structure of La$_5$Ti$_4$O$_{15}$(OH) will be discussed in detail here (Table 1), with crystallographic data of the nearly identical Er$_5$Ti$_4$O$_{15}$(OH) given in the SI (Table SI 1). The unit cell parameters of La$_5$Ti$_4$O$_{15}$(OH) are *a* = 30.516(4) Å, *b* = 5.5837(7) Å , *c* = 7.7593(10) Å, *V* = 1322.1(3) Å^3 and *Z* = 4. Selected bond lengths and bond valence sum calculations are given in the Supporting Information, Tables SI 2 and 4, respectively. The crystal structure of **1** can be best described as a complex three dimensional framework consisting of seven distinct metal sites (five La^{3+} sites and two Ti^{+4} sites), and represents a new structure type, Figure 2. The structural framework consists of La(1)O$_8$, La(2)O$_7$, La(3)O$_8$, La(4)O$_9$ and La(5)O$_9$ coordination environments with La−O bond lengths ranging from 2.360(4) to 2.811(4) Å, and averaging 2.553(4) Å. The LaO$_n$ polyhedra form a three-dimensional (3D) framework built from two unique two-dimensional (2D) La–O–La slabs in the bc plane (Figure 2b). The two unique Ti^{4+} sites both adopt an octahedral geometry

(TiO$_6$) and form their own Ti–O–Ti sublattice of thick 2D slabs along the *bc*-plane (Figure 2c).

The Ti–O–Ti sublattice is embedded inside the 3D La–O–La framework to form a very complex

and dense structure. The Ti–O bond distances range from 1.803(3) to 2.267(3) Å for Ti(1)O$_6$ and

1.827(3) to 2.184(3) Å for Ti(2)O$_6$ showing a highly distorted octahedral environment in both

TiO$_6$ units. The TiO$_6$ octahedra also exhibit angular distortion with *trans*-O–Ti–O angles of

164.21(17)° to 174.99(12)° and *cis*-O–Ti–O angles of 80.12(12)° to 102.72(13)°.
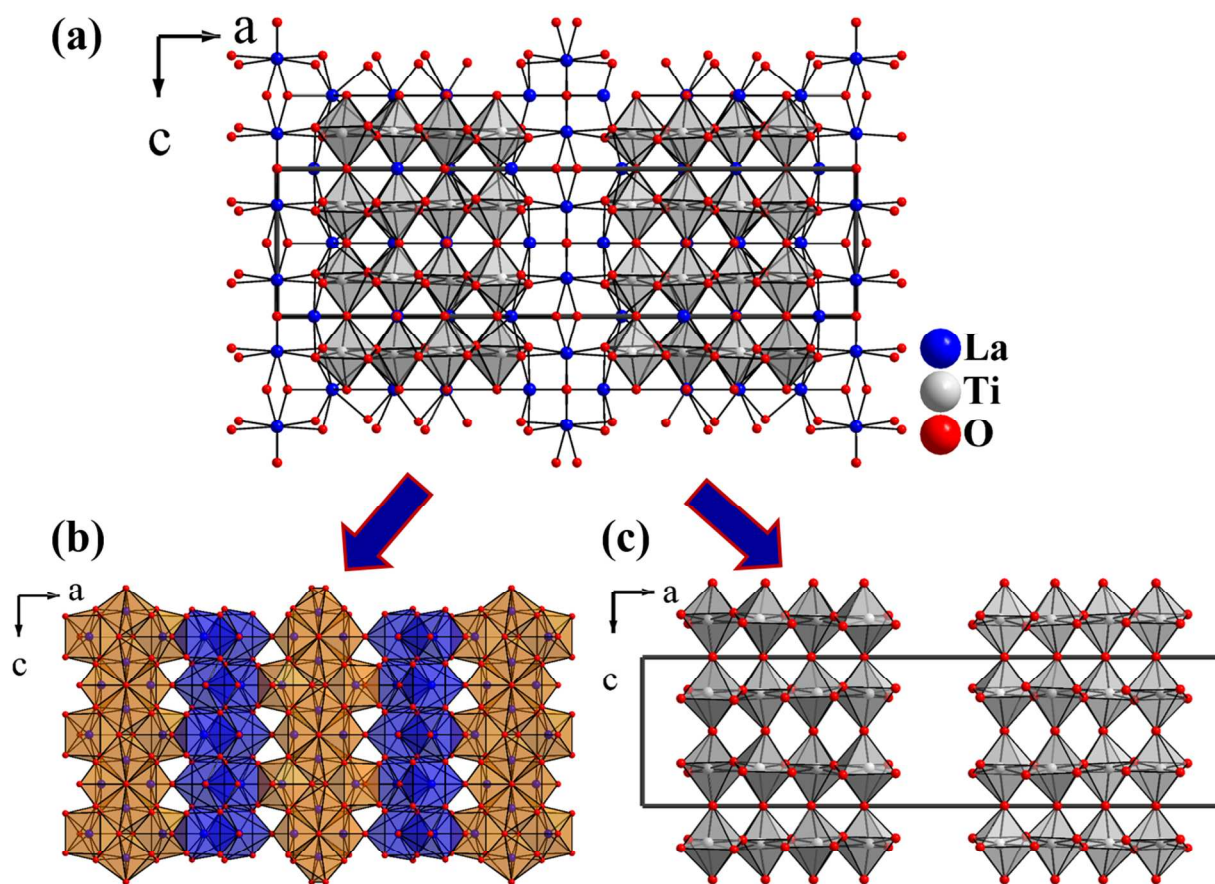
Figure 2. Crystal structure of La$_5$Ti$_4$O$_{15}$(OH) viewing along the *b*-axis. (a) Partial polyhedral view showing the complex nature of the 3D La–O–Ti lattice; (b) Polyhedral view of the 3D La–O–La lattice, where orange and blue colored polyhedra distinguish the two different 2D La–O–La slabs in the *bc* plane, and alternating along the *a*-axis; (c) Construction of the Ti–O–Ti sublattice within the La$_5$Ti$_4$O$_{15}$(OH) unit cell.

The nature of the 3D La–O–La lattice is worth further comment. As shown in Figure 2b, two La–O–La substructures are highlighted using orange (La–O–La slab 1) and blue (La–O–La slab 2) polyhedra and these substructures connect to each other along the a-axis to form the 3D La–O–La lattice where the a-axis is the longest axis in the unit cell (30.516(4) Å). The first sublattice (orange polyhedra in Figure 2b) is formed by La(1)O$_8$, La(2)O$_9$ and La(3)O$_8$ polyhedra. Here, the La(3)O$_8$ polyhedra form edge sharing chains along the c-axis, that are bracketed by the La(1)O$_8$ and La(2)O$_7$ polyhedra also through edge sharing (Figure 3a). Meanwhile, slab 2 is formed by La(4)O$_9$ and La(5)O$_9$ polyhedra connected in alternating, edge sharing fashion as shown in Figure 3b. The overall La–O–La framework is established by corner and edge sharing oxygen atoms joining the slabs along the a-axis. The O(6) oxygen atom was found to be underbonded based on its bond valence sum, as it possesses only three bonds to lanthanum atoms. Electron density in an appropriate geometry for a hydrogen atom attached to O(6) was identified from the difference electron density map, and assigned as such to satisfy the bond valence of O(6) and provide charge neutrality in the structure. The hydrogen atom occupies a small gap in the center of slab 1 of the lanthanum oxide framework. The presence of the OH group was confirmed using single crystal Raman spectroscopy. The Raman spectrum (Figure SI 5) shows OH stretching at 3610 cm^{-1}.
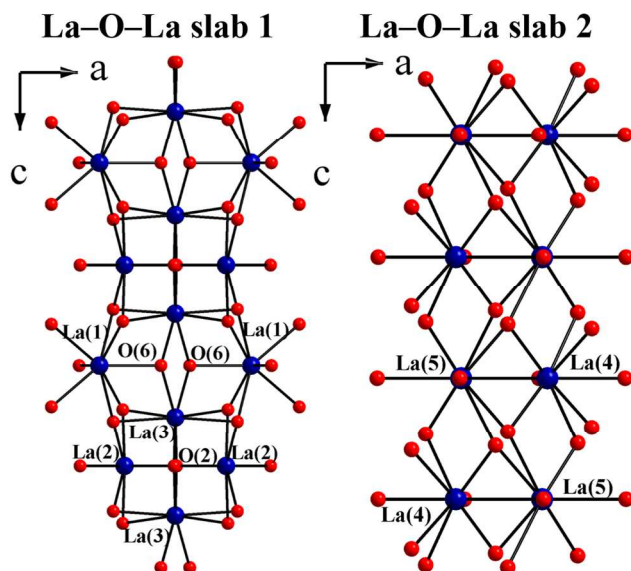
Figure 3. Partial structure of two La–O–La sublattices. Sublattice 1 is formed by La(1)O$_8$, La(2)O$_9$ and La(3)O$_9$ polyhedra and sublattice 2 is formed by La(4)O$_9$ and La(5)O$_9$. These two sublattices interconnect along the *a*-axis to form overall 3D La–O–La lattice.

The structural complexity of this material is also reflected in the titanium environments, Figure 4. Two distinct titanium environments generate a four octahedron thick (along *a*) slab arrangement extending along the *bc*-plane (Figure SI 6) with the thickness seen in the *ac*-plane in Figure 2c and 4. The thick layer is formed by corner sharing Ti(1)O$_6$ and Ti(2)O$_6$ octahedra, defined by intersecting chains of Ti(1)−O(1)−Ti(2)−O(10)−Ti(2)−O(8)−Ti(1) linked in the *ab*-plane, and Ti(1)−O(3)−Ti(1), Ti(1)−O(7)−Ti(1), Ti(2)−O(9)−Ti(2), and Ti(2)−O(11)−Ti(2) connected along *c*-axis, Figure 4b. The complex La–O–Ti framework is formed through a number of edge- and corner-sharing interactions where the Ti–O–Ti and La–O–La sublattices are interpenetrating, Figure SI 7
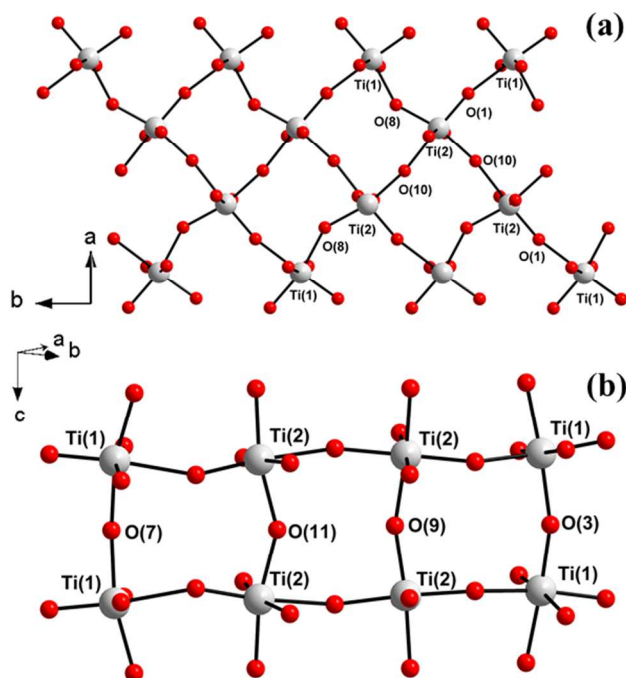
Figure 4. (a) The basic building unit in the Ti–O–Ti lattice along the *ab*-plane ; (b) connectivity between the Ti(1)O_6 and Ti(2)O_6 units within the Ti–O–Ti lattice.

3.3. Crystal Structure of Sm$_3$TiO$_5$(OH)$_3$ II

Compound **II** crystallizes in the monoclinic crystal system in space group $P2_1/m$ with unit cell parameters of a = 5.6066(2) Å, b = 10.4622(4) Å, c = 6.1258(2) Å and β = 104.7390(10)°, V = 347.50(2) Å^3 and Z = 2, Table 1. Sm$_3$TiO$_5$(OH)$_3$ is a titanyl-containing structure type that is a structural analog of other previously reported compounds of formula RE_3MO_5(OH)$_3$ (M = V^{4+}, Ge^{4+}) containing tetravalent building blocks.[62–65] The projection of the structure of Sm$_3$TiO$_5$(OH)$_3$ along *c*-axis is presented in Figure 5. The structure of Sm$_3$TiO$_5$(OH)$_3$ is comprised of two crystallographically distinct SmO$_n$ polyhedra (Sm(1)O$_8$ and Sm(2)O$_7$) and one Ti(1)O$_5$ group. The Sm(1)O$_8$ and Sm(2)O$_7$ units form an interesting 3D rare earth sublattice, Figure SI 8. Herein, Sm(1)O$_8$ and Sm(2)O$_7$ share edges to form chains along the *b*-axis and these chains are interconnected with each other along the *a*-axis to form the 3D Sm–O–Sm sublattice,

Figure SI 8. All oxygen atoms, except O(4) are μ_3 oxo-bridging oxygen atoms within the rare

earth framework, creating numerous triangular lanthanide interactions. Of these oxygen atoms,

O(3) and O(5) do not bridge to the TiO_5 units, and instead support the hydrogen atoms of the

structure. The O(5)-H(5)---O(4) interaction exhibits a favorable distance and geometry for

hydrogen bonding, while the O(3)-H(3) group appears to be a terminal hydroxide ligand. The

hydrogen atom assignments to O(3) and O(5) significantly improves their bond valence sums,

Table SI 5. The Sm−O bond distances range from 2.296(3) to 2.555(3) Å which is consistent

with the analogous germanates and vanadates of this same structure type.[62–65]

The TiO_5 group exhibits a square pyramidal geometry (Figure SI 9) with Ti−O bond

lengths of 1.764(4) Å to the apical O(4) atom and 1.925(3) to 1.944(3) Å to the basal O(1) and

O(2) atoms. The base of the pyramid exhibits some angular distortion, with *cis*-O–Ti–O angles

range from 81.65(16) ° to 86.80(11)°. The apical Ti−O(4) bond in compound **II** exhibits some

titanyl character, and is slightly elongated relative to the titanyl bonds of 1.698(3) Å reported in

$Li_2TiOSiO_4$,[66,67] probably due to the additional bridging nature of O(4) to Sm^{3+} (Sm(1)) in the

present structure. As expected, the Ti−O(4) bond is slightly longer than that of the vanadyl bond

in $Y_3VO_5(OH)_3$ (1.697(5) Å), Table 2. Despite the similarity of the Ti–O and Ge–O apical bond

lengths in the structural analogs (Table 2), there is a much greater difference in apical vs. basal

bond length for the respective MO_5 units in $Sm_3TiO_5(OH)_3$ compared to $Sm_3GeO_5(OH)_3$, also

supporting the concept of a titanyl bond. The corresponding rare-earth vanadates, however,

exhibit a greater degree of $M{=}O$ character using this metric. Although O(4) only possesses bonds

to Ti(1) and Sm(1), it maintains a reasonable bond valence of 1.544 (Table SI 5) given the titanyl

character of the Ti–O(4) bond. The role of O(4) as a hydrogen bond acceptor as described above

further stabilizes this site. The TiO_5 units are isolated relative to one another, but are integrated

into the overall 3D framework by Ti–O–Sm bridging. This occurs by corner-sharing of the apical

oxygen atoms and edge-and corner-sharing of the basal oxygen atoms of the TiO_5 units by Sm

atoms, Figure SI 8.

Table 2. Summary of M=O bond distances for $RE_3MO_5(OH)_3$ (M = V^{+4}, Ge^{+4}, Ti^{+4}).

Structure Type $(RE_3MO_5(OH)_3)$	M=O bond distance (Å)	Average basal oxygen distance (Å)	Δ (basal avg.-M=O) (Å)	Reference
$La_3VO_5(OH)_3$	1.673	1.931	0.258	62
$Dy_3VO_5(OH)_3$	1.670	1.920	0.250	62
$Y_3VO_5(OH)_3$	1.697	1.919	0.222	62
$Sm_3TiO_5(OH)_3$	1.764	1.934	0.170	this work
$Sm_3GeO_5(OH)_3$	1.768	1.863	0.095	65
$Dy_3GeO_5(OH)_3$	1.779	1.860	0.081	64
$Y_3GeO_5(OH_{0.5}F_{0.5})_3$	1.794	1.846	0.052	63
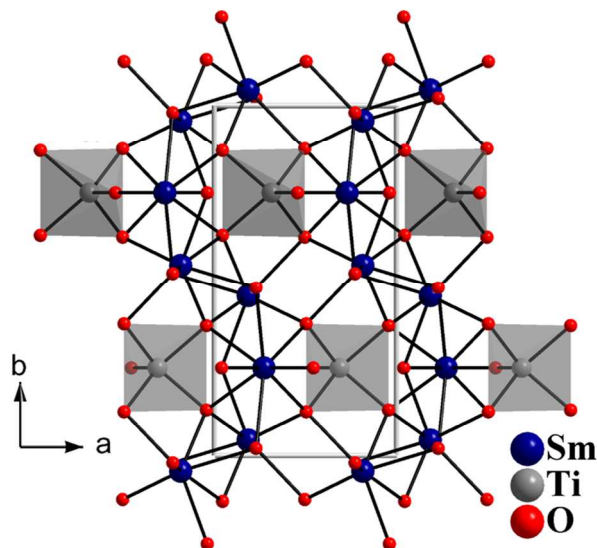
Figure 5. Extended structure of $Sm_3TiO_5(OH)_3$ viewed along [001].

3.4. Crystal structure of $RE_5Ti_2O_{11}(OH)$ (RE = Tm–Lu) III

The crystal structure of $RE_5Ti_2O_{11}(OH)$ (RE = Gd–Lu) type **III**, is monoclinic with $C2/m$ (no. 12) space group symmetry and a = 12.1252(9) Å, b = 5.8243(4) Å, c = 7.0407(5) Å, β = 106.939(3)°, and V = 475.65(6) Å^3. Selected bond lengths and angles are summarized in Table SI 3. Like the previous compounds, $Lu_5Ti_2O_{11}(OH)$ also possesses a complex 3D framework (Figure 6). The rare earth ions form their own 3D framework by edge-shared oxygen atoms. An interesting feature of this rare-earth framework are periodic channels occupied by Ti^{4+}–O–Ti^{4+} chains propagating along the b-axis (Figure 6a, 6b). The chains have alternating short (2.799(8) Å) and long (3.026(8) Å) interatomic distances between Ti^{4+} ions (Figure 6c, and discussion below).

This structure type is analogous with a series of rare-earth containing rhenates, ruthenates, and molybdates, $RE_5M_2O_{12}$ (M = Re, Mo, Ru)[53–56] which are summarized in the SI, Table SI 7. These compounds have been studied due to their interesting magnetic and electric properties.[68] Crystals of these compounds are often reported as twinned and disordered, and compound **III** is also characteristic of these tendencies. The alternating shorter and longer M-M interatomic distances in the previously reported $RE_5M_2O_{12}$ structures were attributed to the formation of M−M bonds along the M−O−M chains, enabled by the presence of unpaired electrons in the extended d orbitals in $4d$ or $5d$ transition metals (molybdenum, rhenium and ruthenium). Indeed this may be the case for these previously reported compounds since they contain open shell d orbitals. The appearance of the shorter Ti−Ti distance in compound **III** however, cannot be justified using the same concept as in the case of $RE_5M_2O_{12}$ compounds. There is no evidence that the metal ions in **III** have anything other than completely empty valence shells. Compound **III** is completely colorless (Figure 1c) which strongly suggests only

the presence of Ti^{4+} since Ti^{3+} is strongly chromophoric. Moreover, lutetium has no reasonable oxidation state other than the empty shell Lu^{3+}, so these factors combine to rule out any electronic effects to cause the shorter titanium distances. Therefore, we can conclude that the alternating distances in **III** are only caused due to the dense packing of the LuO_n polyhedra that form the framework accommodating the chains of TiO_6 octahedra within the unit cell. Furthermore, $Lu_5Ti_2O_{11}(OH)$ exhibits a smaller difference in short versus long M-M distances compared to the Mo, Ru, and Re analogs, where the attractive effects of M-M bond formation are more pronounced. Thus we suggest that the alternating distances in the chains are due in part to some metal–metal interactions when there are open shell valence orbitals, but that these interactions may be encouraged by the packing within the lattice that forces the alternating distances.

The overall Lu–O–Lu lattice is similar to the previously reported $RE_5M_2O_{12}$ structures and it is well discussed in the literature.[69] Charge balance in the $RE_5M_2O_{12}$ (M = Re, Mo, Ru) series is accomplished by mixed-valent M^{4+}/M^{5+} at the transition metal sites. In compound **III**, the presence of the OH stretching vibration at ~3540 cm^{-1} in the Raman spectrum (Figure SI 5) suggests charge balance should be accomplished according to the formula $Lu_5Ti_2O_{11}(OH)$. The O(2) atom was assigned as the OH group on the basis of its lower bond valence sum and its location within the framework capable of sterically supporting the hydrogen atom in ¼ occupancy on the general position.
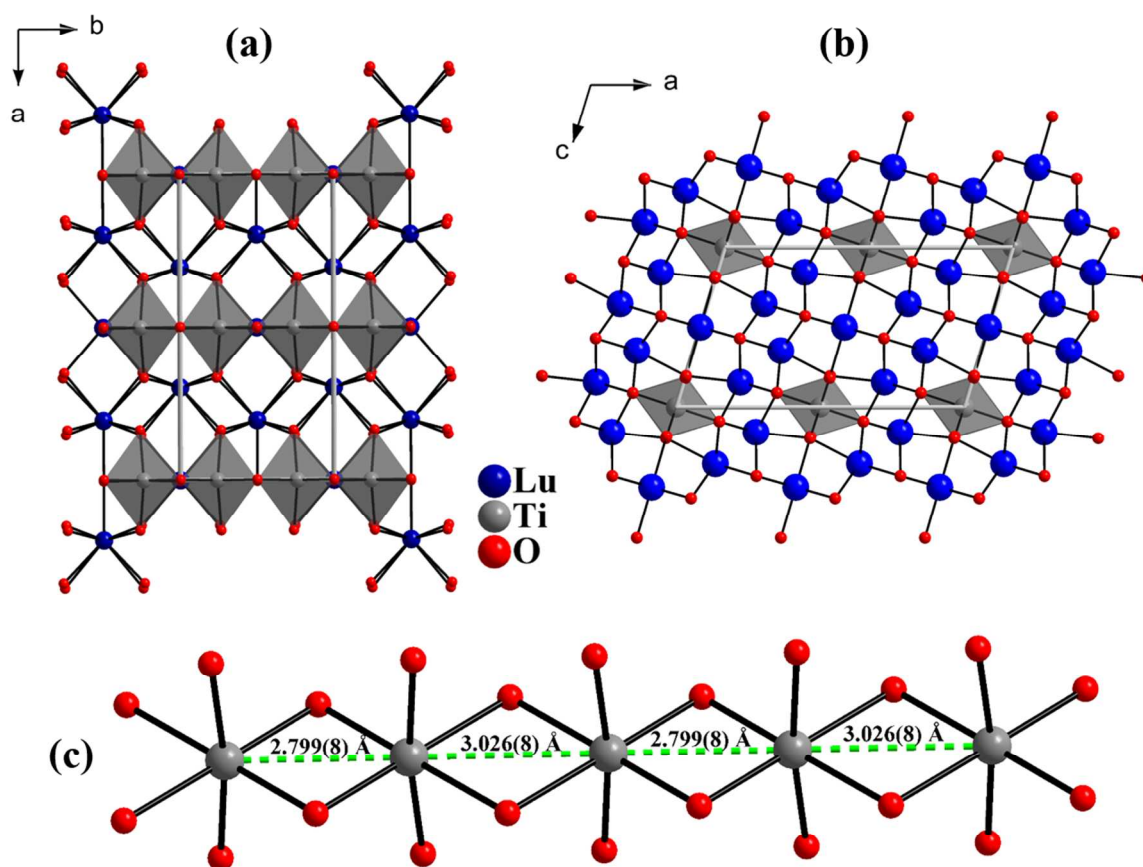
Figure 6. (a) $Lu_5Ti_2O_{11}(OH)$ viewed along [001] direction with infinite titanium oxide chains propagating along the [010] direction; (b) $Lu_5Ti_2O_{11}(OH)$ viewed along [010] direction showing titanium oxide chains occupying channels in the lutetium oxide framework; (c) one dimensional chains of Ti-O-Ti along the b-axis with alternating short and long Ti-Ti distances.

3.5. Crystal structure of Ce$_2$Ti$_4$O$_{11}$ IV

Compound **IV**, Ce$_2$Ti$_4$O$_{11}$, crystallizes in the monoclinic space group $C2/c$ with unit cell parameters of a = 13.6875(7) Å, b = 5.0955(3) Å, c = 12.8592(7) Å, β = 108.964(2)° and V = 848.18(8) Å^3 with Z = 4. The complex 3-D framework features three distinct metal sites, each residing on a general position. Viewed along the b-axis (Figure 7a), the structure can be described as a framework of corrugated 2D layers of cerium and titanium oxides condensed through common oxygen atoms, Figure 7a. Each 2D layer extends in the bc-plane, as shown in Figure 7b and 7c. The cerium oxide sheet is built of one unique Ce atom that is edge- and corner-sharing with neighboring symmetry related Ce sites.   Cerium is in an eight-coordinate environment with Ce−O bond lengths ranging from 2.382(4) to 2.725(4) Å. Two unique titanium atoms, Ti(1) and Ti(2) comprise the titanium oxide layer. The Ti(1) atom adopts a distorted octahedral environment with Ti(1)−O bond distances ranging from 1.879(4) to 2.139(3) Å. The Ti(2) site has a distorted octahedral geometry with an approximate titanyl configuration in which four equatorial Ti(2)−O bonds range from 1.862(4) to 2.068(4) Å, while the opposing axial bonds to oxygen are 1.750(4) Å to O(3) and 2.385(4) Å to O(5) across the 170.13(17)° bond angle.. The two TiO$_6$ distorted octahedra possess a complex connectivity to form Ti–O–Ti 2D layer, as shown in Figure 8. Herein, two Ti(1)O$_6$ octahedra form a dimer by sharing edges via O(4) atoms, while two Ti(2)O$_6$ octahedra form their own dimer through an interesting face sharing connectivity by sharing two O(5) and one O(6) atoms. The respective dimer units share edges with one another, placing O(6) as a common vertex between four Ti atoms as a μ$_4$-oxo bridging atom. The face sharing nature of the two Ti(2)O$_6$ octahedra, brings the two Ti(2) centers into a fairly close proximity of 2.869(2) Å. This structure type was previously reported for Nd$_2$Ti$_4$O$_{11}$,[58] but represents a great expansion of the structurally characterized cerium titanates

beyond $CeTi_2O_6$. The red color of the crystals is likely due to the presence of the f^1 Ce^{3+} ions that are well known to exhibit fully allowed f-d transitions in this spectral region.[70]
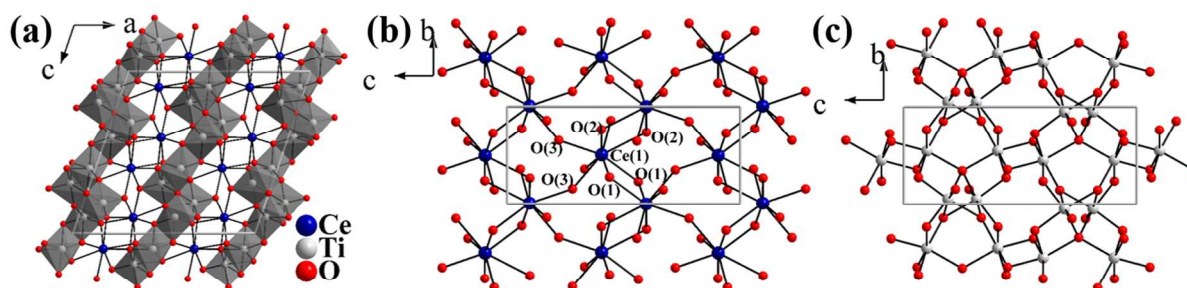
Figure 7. (a) $Ce_2Ti_4O_{11}$ viewed along [010] direction highlighting slabs of alternating rare-earth and titanium oxide polyhedra; (b) the 2D Ce–O–Ce slab in the *bc* plane; (c) the 2D Ti–O–Ti slab in the *bc* plane.
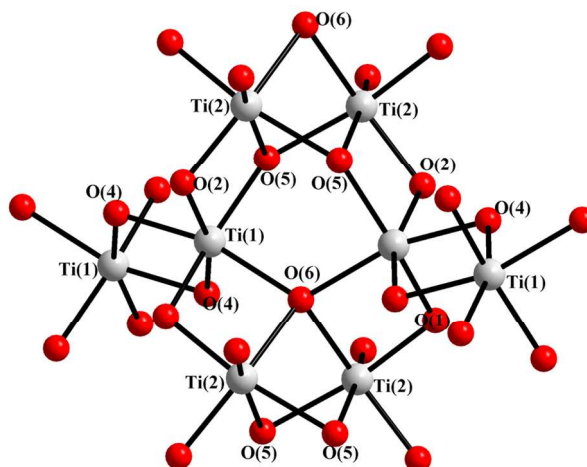
Figure 8. Complex edge-sharing connectivity within the 2D Ti–O–Ti lattice.

4. Conclusions

Systematic exploration of the RE_2O_3-TiO_2 (*RE*=La-Lu) system by high temperature, high pressure hydrothermal synthesis in two different mineralizers reveals a rich chemistry and a variety of structure types across the *f*-block. The descriptive chemistry of rare-earth oxides with titanium oxide is part of a continuing study on the reactivity of refractory oxides in hydrothermal fluids to form interesting new phases, here employing a rational comparison of behavior in

concentrated aqueous hydroxide and fluoride. The identity of various structure types across the f-block ions varies with the nature of this mineralizing fluid and the ionic radius of the rare earth component. The titanium atoms were found to adopt a variety of coordination environments in this study, and the flexibility of Ti^{4+} to adopt octahedral, square pyramidal, or distorted titanyl coordination environments is an additional factor that leads to the variety of structural types. The reduction of Ti^{4+} to Ti^{3+} was not observed in this study in any of the systems we studied.

The ability to mobilize metal oxides into solution by various hydrothermal mineralizers is a vital step for crystal growth. The concentrated hydroxide and fluoride fluids studied here demonstrate the ability to synthesize crystals of new compounds with three dimensional framework structures such as $RE_5Ti_4O_{15}(OH)$ (RE La^{3+}, Er^{3+}), $RE_3TiO_5(OH)_3$ ($RE = Sm^{3+}$), $RE_5Ti_2O_{11}(OH)$ ($RE = Tm^{3+}$-Lu^{3+}), and $Ce_2Ti_4O_{11}$, as well as high quality single crystals of well known cubic ($RE = Gd^{3+}$-Lu^{3+}) and monoclinic ($RE = La^{3+}$, Pr^{3+}, Nd^{3+}) $RE_2Ti_2O_7$-type compounds. Broadly, reactions using the 20 M KOH mineralizer often produced phases that contained hydroxide units in the structure. In marked contrast, the 30 M CsF mineralizer proved useful in accessing anhydrous phases from identical reactions. The complex phase distribution across the f-block, particularly for reactions with aqueous hydroxide, is not yet fully understood. In all cases, it appears that both the refractory rare earth and titanium oxides are readily mineralized and can form mixed oxides. This paves the way for more complex metal oxide combinations, as well as increasingly heavier and more refractory oxides such as the corresponding rare earth zirconates and hafnates, to be investigated.

Conflicts of Interest

The authors declare no conflicts of interest.

Acknowledgement

References

1 M. A. Subramanian, G. Aravamudan and G. V. Subba Rao, *Prog. Solid State Chem.*, 1983, **15**, 55–143.
2 R. Mouta, R. X. Silva and C. W. A. Paschoal, *Acta Crystallogr B*, 2013, **69**, 439–445.
3 J. S. Gardner, M. J. P. Gingras and J. E. Greedan, *Rev. Mod. Phys.*, 2010, **82**, 53–107.
4 S. T. Bramwell, M. N. Field, M. J. Harris and I. P. Parkin, *J. Phys. Condens. Matter*, 2000, **12**, 483.
5 S. T. Bramwell and M. J. P. Gingras, *Science*, 2001, **294**, 1495–1501.
6 T. Fennell, P. P. Deen, A. R. Wildes, K. Schmalzl, D. Prabhakaran, A. T. Boothroyd, R. J. Aldus, D. F. McMorrow and S. T. Bramwell, *Science*, 2009, **326**, 415–417.
7 T. T. A. Lummen, I. P. Handayani, M. C. Donker, D. Fausti, G. Dhalenne, P. Berthet, A. Revcolevschi and P. H. M. van Loosdrecht, *Phys. Rev. B*, 2008, **77**, 214310.
8 O. A. Petrenko, M. R. Lees and G. Balakrishnan, *Phys. Rev. B*, 2003, **68**, 012406.
9 A. P. Ramirez, A. Hayashi, R. J. Cava, R. Siddharthan and B. S. Shastry, *Nature*, 1999, **399**, 333–335.
10 J. Snyder, B. G. Ueland, J. S. Slusky, H. Karunadasa, R. J. Cava and P. Schiffer, *Phys. Rev. B*, 2004, **69**, 064414.
11 M. J. Harris, S. T. Bramwell, D. F. McMorrow, T. Zeiske and K. W. Godfrey, *Phys. Rev. Lett.*, 1997, **79**, 2554–2557.
12 T. Sakakibara, T. Tayama, Z. Hiroi, K. Matsuhira and S. Takagi, *Phys. Rev. Lett.*, 2003, **90**, 207205.
13 B. J. Wuensch, K. W. Eberman, C. Heremans, E. M. Ku, P. Onnerud, E. M. E. Yeo, S. M. Haile, J. K. Stalick and J. D. Jorgensen, *Solid State Ion.*, 2000, **129**, 111–133.
14 P. K. Moon and H. L. Tuller, *Solid State Ion.*, 1988, **28**, 470–474.
15 R. E. Williford, W. J. Weber, R. Devanathan and J. D. Gale, *J. Electroceramics*, 1999, **3**, 409–424.
16 J. M. Farmer, L. A. Boatner, B. C. Chakoumakos, M.-H. Du, M. J. Lance, C. J. Rawn and J. C. Bryan, *J. Alloys Compd.*, 2014, **605**, 63–70.
17 W. J. Weber and R. C. Ewing, *Science*, 2000, **289**, 2051–2052.
18 A. E. Ringwood, S. E. Kesson, N. G. Ware, W. O. Hibberson and A. Major, *Geochem. J.*, 1979, **13**, 141–165.
19 Z. P. Gao, H. X. Yan, H. P. Ning and M. J. Reece, *Adv. Appl. Ceram.*, 2013, **112**, 69–74.
20 H. Yan, H. Ning, Y. Kan, P. Wang and M. J. Reece, *J. Am. Ceram. Soc.*, 2009, **92**, 2270–2275.
21 S. Nanamatsu, M. Kimura, K. Doi, S. Matsushita and N. Yamada, *Ferroelectrics*, 1974, **8**, 511–513.
22 H. W. Schmalle, T. Williams, A. Reller, A. Linden and J. G. Bednorz, *Acta Crystallogr. B*, 1993, **49**, 235–244.
23 M. Tanaka, H. Sekii and K. Ohi, *Jpn. J. Appl. Phys.*, 1985, **24**, 814.

24 F. X. Zhang, J. Lian, U. Becker, R. C. Ewing, L. M. Wang, J. Hu and S. K. Saxena, *J. Solid State Chem.*, 2007, **180**, 571–576.

25 N. Ishizawa, F. Marumo, S. Iwai, M. Kimura and T. Kawamura, *Acta Crystallogr. B*, 1982, **38**, 368–372.

26 V. V. Atuchin, T. A. Gavrilova, J.-C. Grivel, V. G. Kesler and I. B. Troitskaia, *J. Solid State Chem.*, 2012, **195**, 125–131.

27 D. A. MacLean, H.-N. Ng and J. E. Greedan, *J. Solid State Chem.*, 1979, **30**, 35–44.

28 R. D. Aughterson, G. R. Lumpkin, M. de los Reyes, N. Sharma, C. D. Ling, B. Gault, K. L. Smith, M. Avdeev and J. M. Cairney, *J. Solid State Chem.*, 2014, **213**, 182–192.

29 F. X. Zhang, J. W. Wang, M. Lang, J. M. Zhang and R. C. Ewing, *J. Solid State Chem.*, 2010, **183**, 2636–2643.

30 P. Tiedemann and H. Müller-Buschbaum, *Z. Für Anorg. Allg. Chem.*, 1985, **520**, 71–74.

31 S. Hayun and A. Navrotsky, *J. Solid State Chem.*, 2012, **187**, 70–74.

32 P. Konstantinov, K. Krezhov, E. Sváb, G. Mészáros and G. Török, *Phys. B Condens. Matter*, 2000, **276**, 260–261.

33 N. F. Fedorov, O. V. Mel'nikova, V. A. Saltykova and M. V. Chistyakova, *Zhurnal Neorganicheskoj Khimii*, 1979, **24**, 1166–1170.

34 V. Valeš, L. Matějová, Z. Matěj, T. Brunátová and V. Holý, *J. Phys. Chem. Solids*, 2014, **75**, 265–270.

35 T. Hurlen, *Acta Chem Scand*, 1959, **13**, 365–376.

36 R. Feigelson, *50 Years Progress in Crystal Growth: A Reprint Collection*, Elsevier, 2004.

37 C. D. McMillen and J. W. Kolis, *Dalton Trans.*, 2016, **45**, 2772–2784.

38 C. D. McMillen and J. W. Kolis, *Philos. Mag.*, 2012, **92**, 2686–2711.

39 R. A. Laudise, *Prog. Inorg. Chem.*, 1962, **3**, 1–47.

40 K. Byrappa and M. Yoshimura, *Handbook of Hydrothermal Technology*, William Andrew, 2012.

41 C. D. McMillen and J. W. Kolis, *J. Cryst. Growth*, 2008, **310**, 1939–1942.

42 M. Mann and J. Kolis, *J. Cryst. Growth*, 2010, **312**, 461–465.

43 M. Mann, D. Thompson, K. Serivalsatit, T. M. Tritt, J. Ballato and J. Kolis, *Cryst. Growth Des.*, 2010, **10**, 2146–2151.

44 C. A. Moore, C. D. McMillen and J. W. Kolis, *Cryst. Growth Des.*, 2013, **13**, 2298–2306.

45 C. McMillen, D. Thompson, T. Tritt and J. Kolis, *Cryst. Growth Des.*, 2011, **11**, 4386–4391.

46 K. Fulle, C. D. McMillen, L. D. Sanjeewa and J. W. Kolis, *Cryst. Growth Des.*, 2016, **16**, 4910–4917.

47 Apex3; Bruker AXS Inc.: Madison, WI, 2015.

48 G. M. Sheldrick, *Acta Crystallogr. Sect. C Struct. Chem.*, 2015, **71**, 3–8.

49 A. L. Spek, *Acta Crystallogr. D Biol. Crystallogr.*, 2009, **65**, 148–155.

50 N. E. Brese and M. O'Keeffe, *Acta Crystallogr. B*, 1991, **47**, 192–197.

51 I. D. Brown and D. Altermatt, *Acta Crystallogr. B*, 1985, **41**, 244–247.

52 K. Scheunemann and H. Müller-Buschbaum, *J. Inorg. Nucl. Chem.*, 1975, **37**, 2261–2263.

53 M. Bharathy, W. R. Gemmill, A. H. Fox, J. Darriet, M. D. Smith, J. Hadermann, M. S. Remy and H.-C. zur Loye, *J. Solid State Chem.*, 2009, **182**, 1164–1170.

54 L. Chi, J. F. Britten and J. E. Greedan, *J. Solid State Chem.*, 2003, **172**, 451–457.

55 H. Ehrenberg, T. Hartmann, G. Wltschek, H. Fuess, W. Morgenroth and H.-G. Krane, *Acta Crystallogr. B*, 1999, **55**, 849–852.

56 W. Jeitschko, D. H. Heumannskämper, Rodewald Ute Ch. and M. S. Schriewer-Pöttgen, *Z. Für Anorg. Allg. Chem.*, 2000, **626**, 80–88.

57 G. Baud, J.-P. Besse, R. Chevalier and M. Gasperin, *Mater. Chem. Phys.*, 1983, **8**, 93–99.

58 N. Hubner and R. Gruehn, *J. Alloys Compd.*, 1992, **183**, 85–97.

59 L. Kong, D. J. Gregg, E. R. Vance, I. Karatchevtseva, G. R. Lumpkin, M. G. Blackford, R. Holmes, M. Jovanovic and G. Triani, *J. Eur. Ceram. Soc.*, 2017, **37**, 2179–2187.

60 L. Kong, D. J. Gregg, I. Karatchevtseva, Z. Zhang, M. G. Blackford, S. C. Middleburgh, G. R. Lumpkin and G. Triani, *Inorg. Chem.*, 2014, **53**, 6761–6768.

61 C. D. McMillen, S. Comer, K. Fulle, L. D. Sanjeewa and J. W. Kolis, *Acta Crystallogr. Sect. B Struct. Sci. Cryst. Eng. Mater.*, 2015, **71**, 768–776.

62 M. M. Kimani, C. D. McMillen and J. W. Kolis, *Inorg. Chem.*, 2012, **51**, 3588–3596.

63 N. I. Golovastikov and N. V. Belov, *Kristallografiya*, 1982, **27**, 1087–1089.

64 B. F. Mamin, R. A. Khalikov, L. N. Dem'yants, V. M. Golyshev and T. A. Shibanova, *Kristallografiya*, 1987, **32**, 878–881.

65 E. A. Genkina, L. N. Dem'yanets, B. F. Mamin and B. A. Maksimov, *Kristallografiya*, 1989, **34**, 1002–1005.

66 A. Ziadi, G. Thiele, B. Elouadi, *J. Solid State Chem.* 1994, **109**, 112-115.

67 T. J. Bastow, G. A. Botton, J. Etheridge, M. E. Smith, H. J. Whitfield, *Acta Crystallogr. Sect. A* 1999, **A55**, 127-132.

68 C. C. Torardi, C. Fecketter, W. H. McCarroll and F. J. DiSalvo, *J. Solid State Chem.*, 1985, **60**, 332–342.

69 A. J. Cortese, D. Abeysinghe, B. Wilkins, M. D. Smith, G. Morrison and H.-C. zur Loye, *Inorg. Chem.*, 2015, **54**, 11875–11882.

70 P. Dorenbos, *J. Lumin.* 2000, **91**, 155-176.